ORIGINAL PAPER

Meso-scale signatures of inertial transitions in granular materials

A. Clerc[1] · A. Wautier[1] · S. Bonelli[1] · F. Nicot[2]

Abstracts

Granular materials have a complex collective behavior based on simple interactions between grains. The global behavior stems from dynamic rearrangements in the micro-structure. The local increase (resp. decrease) of the density generates jamming (resp. unjamming). In this paper, instabilities in the form of localized bursts of kinetic energy are studied at both the micro-scale (i.e. grain scale) and meso-scale (i.e. cluster scale). The bursts are defined from the variation of kinetic energy. The meso-domains (grain loops in 2D) are built from the tessellation of the medium. We analyze the gain and loss of meso-structures during a localized burst. Surprisingly, micro-structural reorganizations are able to keep the overall statistical equilibrium constant. The introduction of strain-like and stress-like quantities at the mesoscopic scale makes it possible to propose an expression that can be assimilated to mesoscopic second-order work. At this intermediate scale, the negative values of the second-order work are correlated to the appearance of bursts of kinetic energy, which stands for a meso-scale counterpart of Hill's macroscopic criterion of mechanical instability.

Keywords Granular materials · Kinetic energy · Instability · DEM · Meso-scale · Meso-domain

1 Introduction

Granular materials exhibit a complex behavior. A set of solid grains can behave collectively like a solid, in quasi-static regime, or like a fluid, in an inertial regime. Understanding and modeling the diversity of behavior and especially the inertial transition has been an active subject for many years [3, 6, 34]. Inertial transition has a key role to play in the triggering of natural hazards such as landslides or avalanches, or in the failure of civil engineering structures such as earth dams or levees [38]. For such events, bursts of kinetic energy are signatures of mechanical instability and they stand for early clues of inertial transitions [4, 7, 39]. Thus, a close look at these bursts makes a lot of sense to anticipate regime changes in granular materials [8, 13, 26, 33, 40]. Although

these instabilities can have consequences at the macro-scale, they come from sources at the microscopic scale. By looking at small scales, we tend to find precursors to the bursts and identify inertial transition mechanisms. However, it should be emphasized that the constitutive features of granular materials stem from grain rearrangements and subsequent geometrical transformations. Although local behaviour dictates the mutual interaction between contacting particles, mechanisms at the mesoscopic scale are also thought to be very important. As a desire to bridge the gap between constitutive purposes at the macro-scale and elementary considerations at the micro-scale, multi-scale approaches are often considered to study granular materials [11, 15, 16, 31, 42]. Meso-structures such as force chains [27, 28, 33, 37, 38] and grain loops [11, 12, 42] have already proven to be relevant to give information on how forces and geometrical reorganization take place. It is also on a meso-scopic scale that experimental investigations are currently being carried out [2].

In the context of continuum mechanics, including granular materials, instabilities depend on a strain/stress state in comparison with loading conditions. Nicot and Darve [20, 23] have formulated a criterion resuming Hill's sufficient condition of stability (1958). For a material point and for small increments, this criterion reads as follow : "For a given

---

✉ A. Clerc
  adriane.clerc@inrae.fr

1 RECOVER, INRAE, Aix Marseille Univ, 3275 Rte Cézanne, CS 40061, 13182 Aix-en-Provence Cedex 3, France

2 INRAE, ETNA, Université Grenoble Alpes, 2 Rue de la Papeterie BP 76, 38402 Saint Martin d'Hères, France

equilibrium (σ,ε) reached after a given loading history, the material point is unstable if there exists at least one stress increment $\Delta\sigma$, associated with a strain response $\Delta\varepsilon$ such that $\Delta\sigma$:$\Delta\varepsilon<0$". For granular materials, Nicot and Darve [20] have already derived the relationship between kinetic energy variations and the second-order work at the material point scale. In this work, the second-order work is calculated from either macroscopic (stress and strain tensors) quantities or as a summation of local terms built on microscopic quantities (contact forces and inter-granular velocities). The ability of the microscopically defined second-order work to anticipate the occurrence of micro-burst of kinetic energy has been highlighted [4, 20, 36]. However, no works proposed yet a meso-scale definition of the second-order work attached to physical meso-structures relevant to capture the driving elementary mechanisms giving rise to the overall behavior of granular materials.

In this paper, we use meso-domains to study bursts of kinetic energy through numerical simulations based on a discrete element method (DEM) which has proved to be a relevant and powerful tool to study granular material either from a solid or a fluid like point of view [14, 17, 19, 29]. Grain loops are well-defined meso-structures in 2D, but their extension to the 3D case is still an open question [18]. Therefore, DEM simulations are performed in a two-dimensional set up. Inertial transition potentials and consequences at the micro- and macro-scale are examined. The evolution of the second-order work is studied on a mesoscopic scale to link potential instability and inertial transition, which has not yet been done to our knowledge. This paper is organized as follows. In the first section, 2D biaxial tests are presented. In the second section, we analyze the evolution of kinetic energy during the biaxial test. The third section proposes a definition of the meso-structures of interest (namely grain loops), and a rationale formulation of strain and stress increments attached to them. The last section is devoted to the analysis of the results obtained in terms of meso-scale evolutions of micro-structure.

2 Numerical set up

Numerical experiments are carried out with quasi-2D numerical samples using DEM's open-source YADE code [30]. Quasi 2D conditions refer to planar samples composed of spheres, in comparison to the real 2D characterized by planar samples made of discs [9, 32]. Although 3D simulations are possible, meso-structures are, for the moment, only well defined in two-dimensional samples by grain loops [11, 12, 15, 42]. The definition of meso-domains in 3D samples is still an object of research [18] and is out of the scope of this paper.

An idealized granular sample consisting of 25,000 spheres in interaction through an elasto-frictional contact law is considered in this paper (Fig. 1a). The particle
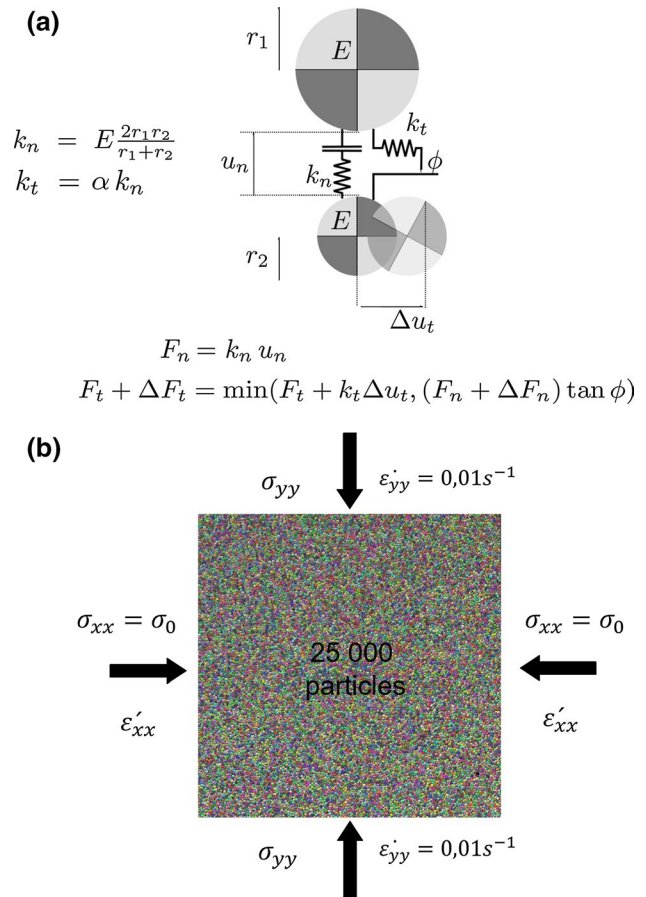

(a)

$$k_n = E\frac{2r_1r_2}{r_1+r_2}$$
$$k_t = \alpha\,k_n$$

$$F_n = k_n\,u_n$$
$$F_t + \Delta F_t = \min(F_t + k_t\Delta u_t, (F_n + \Delta F_n)\tan\phi)$$

(b)

Fig. 1 a Contact law used in discrete element method. The sketch shows the definition of the stiffness coefficients and how the different components of the force contact are calculated. **b** Drained biaxial test: representation of the quasi 2D dense sample of 25,000 spheres and loading conditions

Table 1 Parameters of the numerical simulation

Grain density	3000 kg/m^3
Friction coefficient μ	0.7
k_n/D	356 MPa
k_t/k_n	0.42
Loading rate $\dot{\varepsilon}$	0.01 s^{-1}
Numerical damping coefficient	0.05
D_{max}/D_{min}	3.5
Confining stress σ_0	100 kPa

radii are uniformly distributed with a size ratio D_{max}/D_{min} of 3.5. All sample parameters are recalled in Table 1. The spheres are placed randomly in a square domain which allows working at the material point scale, i.e. at a scale where it is possible to obtain both global (continuum) and local (discrete) views of the granular medium. In order to create a dense sample, the friction coefficient μ
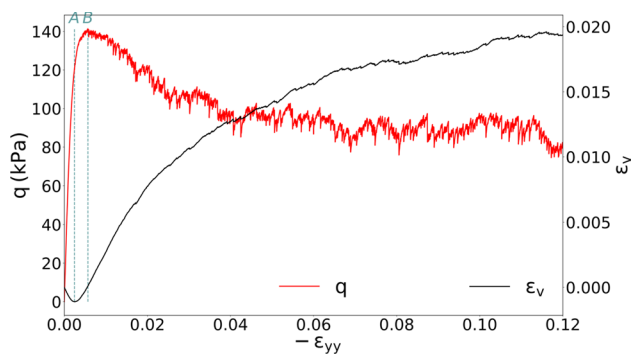
Fig. 2 Deviatoric stress and volumetric strain as a function of the axial strain during the biaxial test

Fig. 3 Evolution of elastic energy E_e, plastic dissipation E_p (left y-axis) and kinetic energy E_c (right y-axis) as a function of the axial strain during the biaxial test. The reference state corresponds to the isotropic compression state reached before the deviatoric loading is applied. State A and B correspond to the characteristic and the peak points shown in Fig. 2. The burst of kinetic energy analysed in this paper corresponds to $-\varepsilon_{yy} = 0.104$ (green dashed line).

at each contact is gradually reduced from 0.7 to 0, while maintaining a pressure of 100 kPa on the lateral boundaries in the preparation step. For a clear understanding of the procedure in quasi 2D, the third and unused dimension of the specimen has been set to one unit length, so that stresses applied on the boundaries can be expressed either in kPa or in N/m simply by dividing the sum of the contact forces by the sample length or width. Numerical damping is chosen low, so as not to inhibit the creation and propagation of kinetic energy bursts Table 1.

The biaxial compression test is broken down into two phases. An isotropic compression of $\sigma_0 = 100$ kPa is firstly applied. The confining pressure σ_0 is then maintained constant on the lateral boundaries while imposing a strain rate $\dot{\varepsilon}$ in the vertical direction (Fig. 1b, Table 1).

The 2D expressions of the deviatoric stress q and the volumetric strain ε_v are

$$q = |\sigma_{yy} - \sigma_{xx}|, \ \varepsilon_v = \varepsilon_{xx} + \varepsilon_{yy} \tag{1}$$

The $q - \varepsilon_{yy}$ curve is typical of the response of a dense sample as shown in Fig. 2, where the vertical lines A and B represent respectively the characteristic point of the volumetric strain ε_v and the maximum of the deviatoric stress q. The curve shows a hardening regime represented by a strong increase leading to a peak, then a softening regime takes place, with a small decrease of the deviatoric stress followed by a plateau. Here the q peak is obtained at less than 1% of the axial strain (line B in Fig. 2). An early q peak is often found with numerical simulations compared to experimental simulations, which is attributed to the use of the perfect spheres in DEM instead of irregular shapes as with real particles. The ε_v curve is also characteristic of a dense material with, firstly, a small compression behavior, the maximum of which is reached before the q peak (vertical line A in Fig. 2), and secondly, a dilation until the end of the test.
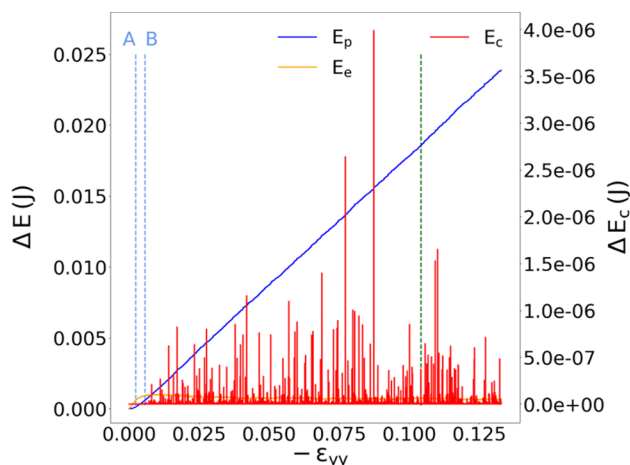
3 Analysis of bursts of kinetic energy

Using numerical simulation, the data can be analyzed either at the whole sample level or at the grain or cluster scale. Figure 3 shows the changes in elastic, plastic and kinetic energies as a function of axial strain during the biaxial test. Kinetic energy is represented with a different scale to highlight the frequency of large variations. In Fig. 3, dashed blue vertical lines highlight the occurrence of the bursts studied in this paper given by:

$$E_c^g = \tfrac{1}{2} m_g ||\mathbf{c}_g||^2 + \tfrac{1}{5} m_g |\omega R_g|^2 \tag{2}$$

where m_g is the grain mass, R_g is the grain radius, $\mathbf{c}_g$ and are the translation velocity vector and the rotation velocity of the grain, respectively.

For elasto-frictional contacts (Fig. 1a), the stored elastic energy of a contact is

$$E_e^g = \tfrac{1}{2} k_n (u_n^c)^2 + \tfrac{1}{2} k_t ||\mathbf{u}_t^c||^2 = \tfrac{1}{2} k_n^{-1} (F_n^c)^2 + \tfrac{1}{2} k_t^{-1} ||\mathbf{F}_t^c||^2 \tag{3}$$

where and are the normal and tangential stiffnesses, and the normal and tangential relative displacements at contact, and are the normal and tangential contact forces.

When contact sliding occurs ($\mathbf{F}_t^c = \mu F_n^c$) some energy is dissipated. A non-reversible tangential displacement velocity generates a positive plastic dissipation

$$\dot{E}_p^c = \mathbf{F}_t^c \cdot \dot{\mathbf{u}}_t^c \tag{4}$$

From the Eqs. (2)-(4), energy variations at the sample scale during the deviatoric loading over a given time range
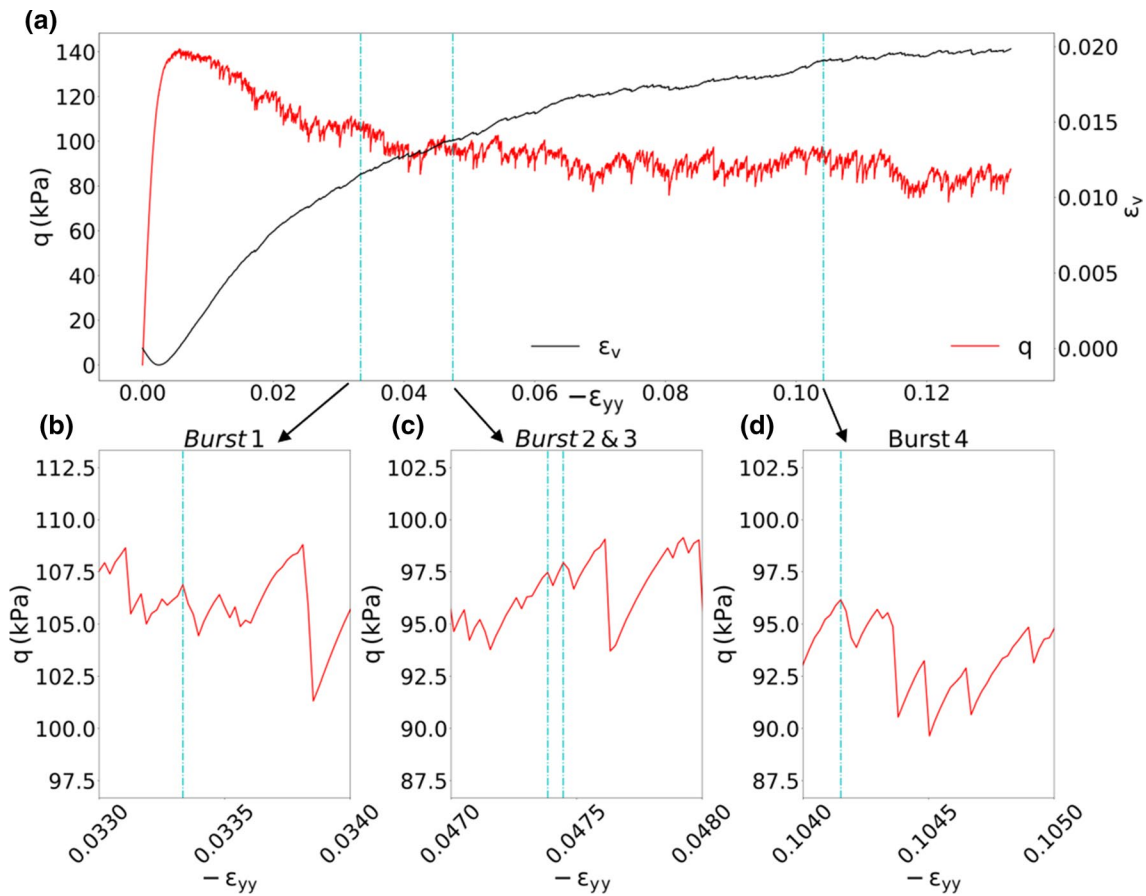
Fig. 4 Analysis of the four bursts considered in the manuscript, in terms of deviatoric stress q evolution during the biaxial test. The vertical lines correspond to the beginning of bursts

$[t_0, t]$ are obtained by summing the kinetic energy on the grains, and by summing the elastic energy E_e and the plastic dissipation E_p on the contacts:

$$\Delta E_c(t) = \sum_g E_c^g(t) - E_c^g(t_0), \Delta E_e(t)$$

$$= \sum_c E_e^c(t) - E_e^c(t_0), \Delta E_p(t) = \int_{t_0}^{t} \sum_c \dot{E}_e^c(t') dt' \qquad (5)$$

Local outbursts of kinetic energy are detected if the kinetic energy of a part of the sample is greater than the mean kinetic energy. The overall kinetic energy of the sample is of the order of 10^{-8} J. The mean kinetic energy of a grain (out of 25,000) is therefore of the order of 10^{-13} J. As shown in Fig. 3, there are many important variations from the mean value. Four bursts of kinetic energy are chosen and studied (Fig. 4). They occur on the plateau (Fig. 4a) where a quasi-stationary regime corresponding to the so-called 'critical state' is reached (state at which a granular material can be continuously sheared under a constant mean pressure without any change in volume). A close look on the

deviatoric stress curve around the appearance of the bursts is provided in Fig. 4b–d. This highlights the fact that the onset of each burst corresponds to a drop in q. A localized explosion of kinetic energy has thus some macroscopic consequences in the form of a small transient instability. Burst No.2 and No.3 were initially detected as a single burst, but after a more detailed examination, they appeared to be two consecutive bursts that propagate in slightly different areas.

For the sake of clarity, only burst No.4 is investigated in the following. All the presented results are similar for other bursts. Figure 5 shows a reduced time lapse for the burst 4. It highlights the typical onset and evolution of kinetic bursts of energy observed on the constant plateau of a drained biaxial test. In Fig. 5, grains that have a kinetic energy at least twice the mean kinetic energy of a grain are highlighted. From a state where most grains have a low kinetic energy (less than the mean kinetic energy of a grain), the initiation affects only a few grains, before spreading to nearly half of the sample and disappearing. In its initiation, propagation and attenuation, the center of the burst moves slightly in the positive direction of x-axis, but the set of grains with large kinetic
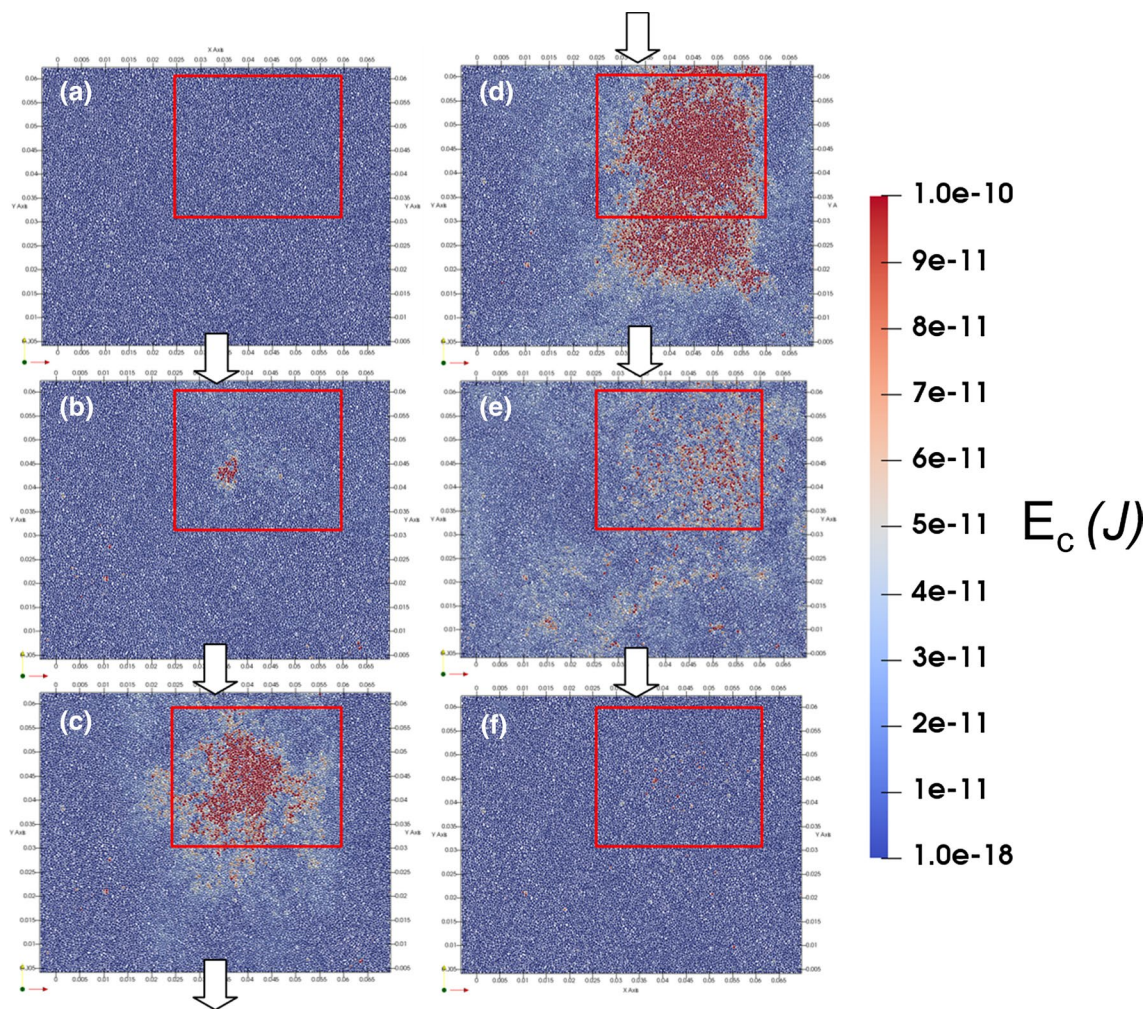
Fig. 5 Reduced time lapse of the burst of kinetic energy No.4. Particles are coloured according to their kinetic energy (in Joule). The bounding box used to provide an approximate definition of the burst domain is shown in red

energy remains limited and the burst does not propagate to the whole sample, as it could be observed in case of material instability [39].

To better understand the mechanisms that trigger a burst and drive its propagation, we need to distinguish the area where the burst occurs and propagates from the rest of the sample domain. This is done with use of a fixed box defined around the burst, considering the location of the start and the direction of propagation (Fig. 5c). On the Fig. 5c, the box is displayed, showing a rectangle of dimensions [0.03 m, 0.032 m] centered on the point (0.045 m, 0.046 m). The same energy variation analysis as in Fig. 3 at the scale of the defined box is reported in Fig. 6. The energy variations show that, when the kinetic energy breaks up (vertical lines), the kinetic energy passes through a peak, while the elastic energy decreases, and the plastic energy increases (Fig. 6). On the basis of these variations, it is concluded that there is an excess of elastic energy stored in the contacts,

which is then transformed into kinetic energy (the grains move linearly or rotate) and dissipated by friction (corresponding to a slip between the grains in the contacts). However, the variations in kinetic energy are very small compared with the variations in plastic energy. Frictional dissipation is thus the main mechanism active during the burst of kinetic energy. Kinetic energy, which is the easiest signature of local instabilities, represents indeed only a small part of the energy transfer from the elastic energy for kinetic outbursts occurring at critical state in drained biaxial tests. It should be underlined that this analysis depends on the contact friction. In the two extreme cases of frictionless grains ($\mu = 0$) of fully elastic contacts ($\mu = +\infty$), no plastic dissipation can occur, and the elastic energy transforms entirely into kinetic energy. However, for intermediate friction (corresponding to more realistic materials), and for similar stress levels, the above analysis holds with dissipative mechanisms being prominent.
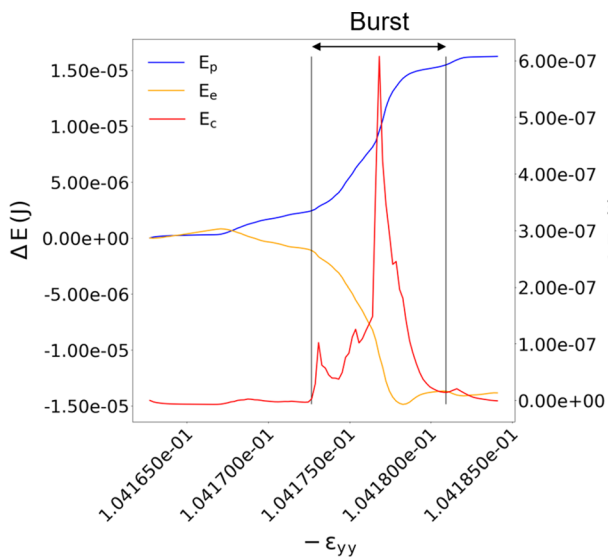
Fig. 6 Evolution of the plastic dissipation E_p, of the elastic energy E_e (left y-axis), and of the kinetic energy E_c (right y-axis) during the burst of kinetic energy No. 4

These energetic considerations are only a first step towards understanding the origins of bursts. Additional parameters are required to investigate the location of the burst in a specific area. The sliding index for each contact is defined as follows:

$$I_p = \frac{||\mathbf{F}_t||}{\mu |F_n|} \tag{6}$$

This index, belonging to the [0,1] interval, is an indicator of the potential instability of a contact (the value 1 corresponding

to contact sliding). The probability density of I_p for contacts inside and outside the kinetic energy burst zone is given in Fig. 7. Before the burst (Fig. 7a), a larger fraction of the contacts is close to sliding (I_p close to 1) in the burst domain than outside. After the occurrence of the burst (Fig. 7b), no unstable contacts remain in the burst domain (the tail of the I_p probability density function inside the burst domain converges to the one out of the burst domain). The probability curve outside the zone does not change much. I_p close to 1 is a necessary condition to observe a burst of kinetic energy. Similar findings were obtained by Wautier et al. [39].

This last result reinforces the delineation of the burst zone and provides clues to relate the burst spatial extension to some underlying microstructure characteristics. There is a strong contrast between the behavior of grains inside and outside of the area. The burst is likely to be rooted in a zone with high level of stored elastic energy and high concentration of unstable contacts. The analysis will now be carried out on a mesoscopic scale, which requires the definition of relevant mechanical quantities at this scale.

4 Definition of quantities at the mesoscopic scale

4.1 Definition of meso-domains

In order to define clusters of grains, a convenient method in 2D is to tesselate the sample area with grain loops. As a result, the sample domain can be seen as the union of loops involving a variable number of grains. Recent studies have shown the relevance of defining such a meso-scale based on
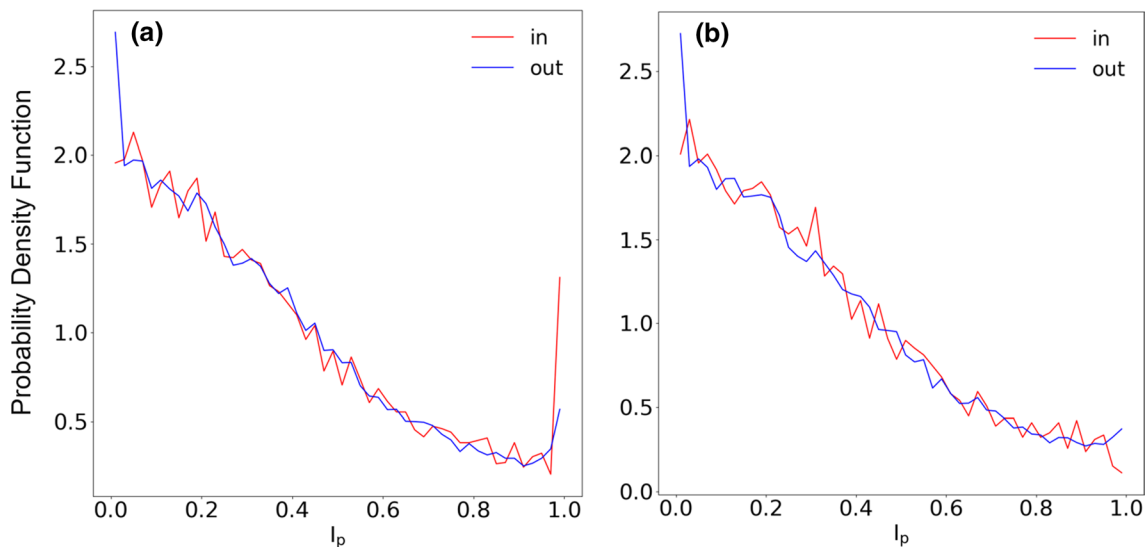

Fig. 7 Sliding index's probability density before (**a**) and after (**b**) the burst of kinetic energy inside (red) and outside (blue) the surroundings of the burst area
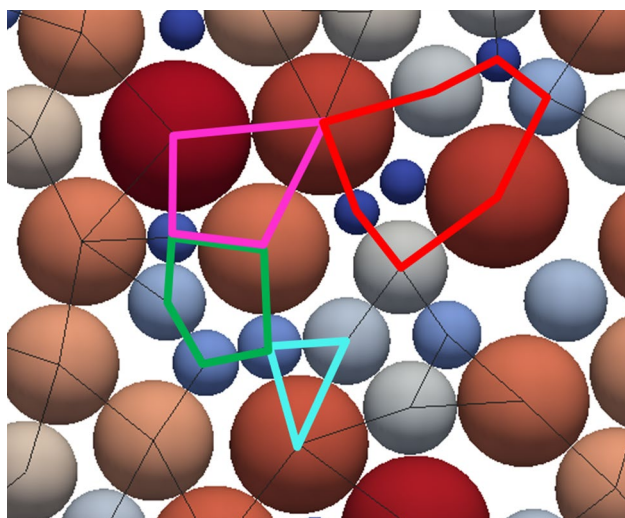
Fig. 8 Insight of the tessellation of the sample domain into loops. Focus on four loops of different order (L3, L4, L5 and L6)

grain loops to characterize changes in the micro-structure of granular materials [15, 42, 11].

A unique tessellation is obtained, with loops of order 3, 4, 5 and 6+ according to the number of spheres they contain (Fig. 8 show a small portion of the tessellation). The loop porosity is expected to increase with the loop order. Thus, lower order loops are on average less deformable than higher order loops. Grain loops play a key role in the reorganization of the micro-structure, as a means of adapting to external loadings. Non-contact or single-contact grains, called rattlers, are visible inside the high-order loops in Fig. 8. They are also good indicators of reorganization since they are created from broken meso-structures and they can be trapped in meso-structures under construction.

4.2 Definition of a mesoscopic second-order work

The ability of a system to develop kinetic energy with no external disturbance from an equilibrium state[1] is described by the balance equation of second-order works

$$2E_c(t + \triangle t) = W_2^{ext} - W_2^{int} \tag{7}$$

$$W_2^{ext} = \int_{\partial\Omega} \triangle \mathbf{f} \cdot \triangle \mathbf{u} dA, \quad W_2^{int} = \int_{\Omega} \triangle \boldsymbol{\sigma} : \triangle \boldsymbol{\varepsilon} dV \tag{8}$$

where E_c represents the overall kinetic energy, W_2^{ext} is the external second-order work, W_2^{int} is the internal second-order

_____

[1] An equilibrium state is characterized by a nil kinetic energy, and by the fact that any variation of energy from the current state is a second order function of the applied perturbation.

work, $\mathbf{f} = \boldsymbol{\sigma} \cdot \mathbf{n}$ and $\mathbf{u}$ denote the stress and displacement vectors on $\partial\Omega$, $\boldsymbol{\sigma}$ and $\boldsymbol{\varepsilon}$ denote the stress and strain tensors in Ω, and $\triangle$ is the increment between times t and $t + \triangle t$.

There are two requirements for using second-order work criteria for a stability analysis:

–this criterion is most often used when the system control parameters are kept constant, or $\triangle \mathbf{f} \cdot \triangle \mathbf{u} = 0$ on $\partial\Omega$, to highlight situations where the deformation of the system can be carried on without any input of external energy;

–the system must be in balance initially ($E_c(t) = 0$). As $W_2^{ext} = 0$, the system evolves from a static situation to a inertial regime ($E_c(t + \triangle t) > 0$) is only if $W_2^{int} < 0$. Therefore, Eq. (8) does not apply once the system is out of equilibrium.

There is a priori no reason for the selected meso-domains to check these two conditions. Despite these restrictions, we propose to define adequate quantities $\boldsymbol{\sigma}_{\Omega_l}$ and $\boldsymbol{\varepsilon}_{\Omega_l}$, corresponding to stresses and strains in a mesoscopic domain $\Omega_l(t)$, and to analyze the evolution of a so-called mesoscopic second-order work

$$(W_2)_{\Omega_l} = \langle \triangle \boldsymbol{\sigma} \rangle_{\Omega_l} : \langle \triangle \boldsymbol{\varepsilon} \rangle_{\Omega_l} \tag{9}$$

This approach assumes that the Macro-Homogeneity condition (second-order Hill-Mandel lemma) is respected on the domain Ω:

$$\langle \triangle \boldsymbol{\sigma} : \triangle \boldsymbol{\varepsilon} \rangle_\Omega = \langle \triangle \boldsymbol{\sigma} \rangle_\Omega : \langle \triangle \boldsymbol{\varepsilon} \rangle_\Omega, \langle \cdot \rangle_\Omega = \frac{1}{|\Omega|} \int_\Omega \cdot dV \tag{10}$$

The necessary conditions to ensure the validity of this second-order Hill-Mandel lemma has been discussed in details in [22]. Such a relationship has not yet been discussed for mesoscopic quantities, for which the domain Ω cannot be considered as a representative elementary volume. Therefore, the specific form of equation (7) at the mesoscale remains to be discussed. Such an analytical discussion is saved for future investigations as it is out of the scope of the present paper.

4.3 Definition of the mesoscopic incremental strain

The average strain rate $\langle \boldsymbol{\varepsilon} \rangle_{\Omega_l}$ on a domain Ω_l is completely defined in terms of quantities on the boundary $\partial\Omega_l$ as follows:

$$\langle \boldsymbol{\varepsilon} \rangle_{\Omega_l} = \frac{1}{|\Omega_l|} \int_{\partial\Omega_l} \mathbf{u} \otimes_s \mathbf{n} dA \tag{11}$$

where $\mathbf{u}$ is the displacement vector, $\mathbf{n}$ is the outer normal to Ω_l, and $\otimes_s$ denotes the symmetric tensor product ($\mathbf{u} \otimes_s \mathbf{n} = \frac{1}{2}(\mathbf{u} \otimes \mathbf{n} + \mathbf{n} \otimes \mathbf{u})$). The analysis of kinetic energy at the microscopic scale is carried out in very small-time steps Δt. It is therefore relevant to assume that the system undergoes small perturbations between $\Omega_l(t)$, and $\Omega_l(t + \Delta t)$.
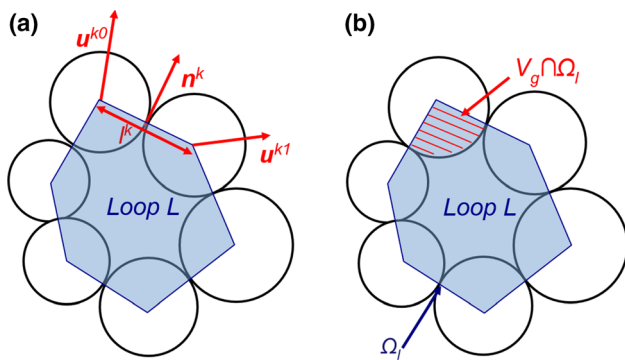
Fig. 9 Sketch of the calculation of the strain (**a**) and stress (**b**) defined at the scale of a meso-domain

This point is debatable though and will have to be considered by further research.

The incremental meso-strain between time t and $t+\Delta t$ can be expressed by means of the incremental displacement vector $\Delta \mathbf{u} = \mathbf{u}(t + \Delta t) - \mathbf{u}(t)$:

$$\langle \Delta \boldsymbol{\varepsilon} \rangle_{\Omega_l} = \frac{1}{|\Omega_l|} \int_{\partial \Omega_l} \Delta \mathbf{u} \otimes_s \mathbf{n} dA \tag{12}$$

where Ω_l and $\mathbf{n}$ are considered at time t. As the domain Ω_l is updated at each increment, it is an updated Lagrangian description which allows large strains at the mesoscopic level over a large number of time steps.

A grain loop is delimited by branch vectors joining the center of neighbor spheres (Fig. 9a). This is the polygon on which the meso-strain calculations are based. The meso-strain tensor as a grain loop quantity can be expressed as a function of a linear interpolation of the incremental displacements of the peripheral grains [15, 1]:

$$\langle \Delta \boldsymbol{\varepsilon} \rangle_{\Omega_l} = \frac{1}{|\Omega_l|} \sum_{k \in \partial \Omega_l} \frac{1}{2}(\Delta \mathbf{u}_k^0 + \Delta \mathbf{u}_k^1) \otimes_s \mathbf{n}_k l_k \tag{13}$$

where $\mathbf{u}_k^0$ and $\mathbf{u}_k^1$ are the incremental displacement vectors of the vertices of the kth edge (grains centers), l_k is the length of the kth edge, and $\mathbf{n}_k$ is the normal to the kth edge (outer to Ω_l).

4.4 Definition of the mesoscopic incremental stress

For the stress tensor, deriving an incremental formulation is more complex than it might appear at first glance. Indeed, defining a meso-stress is relatively simple with use of Love-Weber or Bagi formulas [1, 21, 41], but an incremental formulation requires that the loops are not reorganized between two close configurations. To address this issue, we are looking for a definition of incremental meso-stress based on the incremental stresses in the grains. The meso-stress is expressed as the spatial average on Ω_l of the micro-stress (Fig. 9b):

$$\langle \boldsymbol{\sigma} \rangle_{\Omega_l} = \frac{1}{|\Omega_l|} \int_{\Omega_l} \boldsymbol{\sigma} dV \tag{14}$$

As the local stress tensor $\boldsymbol{\sigma}$ is equal to zero in empty space, the integral can be transformed into a sum over the portions of the spheres included in Ω_l, noted $V_g \cap \Omega_l$:

$$\langle \boldsymbol{\sigma} \rangle_{\Omega_l} = \frac{1}{|\Omega_l|} \sum_{g \in \partial \Omega_l} \int_{V_g \cap \Omega_l} \boldsymbol{\sigma} dV \tag{15}$$

By introducing the average stress on the parts of the spheres included in Ω_l, noted $\langle \boldsymbol{\sigma} \rangle_{V_{g \cap \Omega_l}}$, it comes

$$\langle \boldsymbol{\sigma} \rangle_{\Omega_l} = \frac{1}{|\Omega_l|} \sum_{g \in \partial \Omega_l} |V_g \cap \Omega_l| \langle \boldsymbol{\sigma} \rangle_{V_g \cap \Omega_l} \tag{16}$$

In addition, if the average stress calculated on the part of the spheres included in the loop is assumed to be equal to the average stress of the grain: $\langle \boldsymbol{\sigma} \rangle_{V_{g \cap \Omega_l}} = \langle \boldsymbol{\sigma} \rangle_{V_g}$, the meso-stress is then proportional to the sum of the grains stress weighted by their volume fraction in Ω_l (Fig. 9b):

$$\langle \boldsymbol{\sigma} \rangle_{\Omega_l} = \frac{1}{|\Omega_l|} \sum_{g \in \partial \Omega_l} |V_g \cap \Omega_l| \langle \boldsymbol{\sigma} \rangle_{V_g} \tag{17}$$

Although the grains are assumed rigid in DEM, they are subject to a local stress $\boldsymbol{\sigma}$, which is a symmetrical second-order tensor and verifies the equation of motion $\rho \ddot{x} = \text{div}(\boldsymbol{\sigma})$ and $\boldsymbol{\sigma} = \boldsymbol{\sigma}^T$. Thus, in dynamic evolution, the average stress $\langle \boldsymbol{\sigma} \rangle_{V_g}$ is equal to

$$\langle \boldsymbol{\sigma} \rangle_{V_g} = \frac{1}{|V_g|} \int_{\partial V_g} \boldsymbol{\sigma} \cdot \mathbf{n} \otimes_s (\mathbf{x} - \mathbf{c}_g) dA + \frac{1}{|V_g|} \int_{V_g} \rho \ddot{\mathbf{x}} \otimes_s (\mathbf{x} - \mathbf{c}_g) dV \tag{18}$$

The grain is only subjected to punctual contact forces vectors $\mathbf{f}_c$ on ∂V_g, therefore, the left-hand side term of Eq. (18) is equal to

$$\frac{1}{|V_g|} \int_{\partial V_g} \boldsymbol{\sigma} \cdot \mathbf{n} \otimes_s (\mathbf{x} - \mathbf{c}_g) dA = \frac{D_g}{2|V_g|} \sum_{c \in \partial V_g} \mathbf{f}_c \otimes_s \mathbf{n}_c \tag{19}$$

where the index c runs through all contacts of the grain g, D_g is the grain diameter, and $\mathbf{n}_c$ is the outer normal to V_g at contact c.

The kinematics of the rigid grain is described by $\dot{\mathbf{x}} = \dot{\mathbf{c}}_g + \mathbf{Q}_g \cdot (\mathbf{x} - \mathbf{c}_g)$ for any $\mathbf{x} \in V_g$, where $\mathbf{c}_g$ is the grain center, and $\mathbf{Q}_g$ is the second-order skew-symmetric tensor describing the grain rotation. Therefore, the second right-hand side term of Eq. (19) is equal to

$$\frac{1}{|V_g|} \int_{V_g} \rho \ddot{\mathbf{x}} \otimes_s (\mathbf{x} - \mathbf{c}_g) dV = \frac{\rho D_g^2}{10}(\dot{\mathbf{Q}}_g + \mathbf{Q}_g^2) \tag{20}$$

as $\ddot{x} = \ddot{c}_g + \left(\dot{\mathbf{Q}}_g + \mathbf{Q}_g^2 \right) \cdot \left(\mathbf{x} - \mathbf{c}_g \right)$ It is assumed here that the contribution of grain rotation is negligible compared to the contribution of contact forces. This is justified by the fact that the ratio between rotation term Eq. (20) and contact force term Eq. (19) scales with D_g^4. Nevertheless, since contact forces are likely to become very weak during a burst of kinetic energy, this point is debatable and will have to be verified by further research.

Finally, the expression of the meso-stress is of a form similar to, but different from the Love-Weber formula for the set of grains concerned:

$$\langle \boldsymbol{\sigma} \rangle_{\Omega_l} = \frac{1}{|\Omega_l|} \sum_{g \in \partial \Omega_l} \frac{D_g |V_g \cap \Omega_l|}{2|V_g|} \sum_{c \in \partial V_g} \mathbf{f}_c \otimes_s \mathbf{n}_c \tag{21}$$

This difference is due to the fact that the domain Ω_l is defined by the centers of the grains and does not contain the entire volume of grains. This definition is similar but not identical to that of Liu et al [12]. Moreover, this expression is not restricted to a quasi-static evolution and can be extended to dynamical situations when the contribution of rotations given by Eq. (20) is non-negligible. Note that Eq. (18) is consistent with the macro-stress definition computed at the scale of the sample Ω:

$$\langle \boldsymbol{\sigma} \rangle_{\Omega} = \frac{1}{|\Omega|} \int_{\Omega} \boldsymbol{\sigma} dV = \frac{1}{|\Omega_l|} \sum_{g \in \partial \Omega} |V_g| \langle \boldsymbol{\sigma} \rangle_{V_g}$$
$$= \frac{1}{|\Omega_l|} \sum_{l} \sum_{g \in \partial \Omega_l} |V_g \cap \Omega_l| \langle \boldsymbol{\sigma} \rangle_{V_g} = \frac{1}{|\Omega_l|} \sum_{l} |\Omega_l| \langle \boldsymbol{\sigma} \rangle_{\Omega_l} \tag{22}$$

The hypothesis of small geometric transformations between times t and $t+\Delta t$ allows to suppose that

$$\langle \Delta \boldsymbol{\sigma} \rangle_{\Omega_l} = \Delta \langle \boldsymbol{\sigma} \rangle_{\Omega_l} \tag{23}$$

Thus, the incremental meso-stress between time t and $t+\Delta t$ is now simply defined as follows

$$\langle \Delta \boldsymbol{\sigma} \rangle_{\Omega_l} = \langle \boldsymbol{\sigma}(t + \Delta t) \rangle_{\Omega_l} - \langle \boldsymbol{\sigma}(t) \rangle_{\Omega_l} \tag{24}$$

where Ω_l is considered at time t. As the domain Ω_l is updated at each increment, it is an updated Lagrangian description.

5 Analysis of the changes at the mesoscopic scale during the outburst of kinetic energy

5.1 Evolution of meso-structures during the burst of kinetic energy

The ratio of each loop category (L3, L4, L5, L6+) depends on the nature of the sample and the loading history. In Fig. 10, the evolution of the loop ratios along a biaxial test
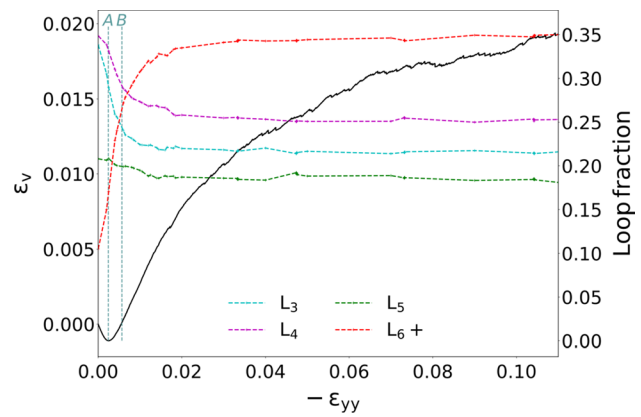

Fig. 10 Evolution of loop fractions as a function of the axial strain during the biaxial test. The macroscopic volumetric strain is recalled in black. The characteristic point (A) and stress peak (B) defined in Fig. 2 are shown with vertical dashed lines

is given against the volumetric strain. Before maximum contractancy (vertical line A in Fig. 4, low order loops are the majority (about 70% of loops of order 3 and 4), and loops of order 6 or higher are the minority (between 10 and 15% of the total fraction of the loop). However, from the maximum deviatoric stress state (vertical line B in Fig. 4), loops of order higher than 6 are more numerous than those of lower order, while the fraction of loops of order 5 remains stable. Referring to Liu et al. [11], two distinct evolutions can be envisaged for dense sample when a strain localization develops. In the present biaxial test, no strain localization is observed. As a result, it is observed that the final proportion of loops found in at the steady-state are very similar to those reported in Liu et al. [11] when restricting the analysis to the shear band domain only. With the help of Fig. 2, we can also interpret this evolution from less deformable loops to more deformable loops as a mesoscopic equivalent of the macro-evolution of the volumetric strain: the appearance of the dilatancy goes hand in hand with the increase of the fraction of loops that contain more void.

The evolution rate of grain loops and rattlers are now studied during the burst of kinetic energy, inside and outside the burst zone. The relative evolution of the number of loops is equal to $\frac{N_t - N_{t+dt}}{N_0}$ where N_t (resp N_{t+dt}) is the number of loops at time t (resp $t+dt$), and N_0 the total number of loops in the domain at the beginning of the numerical recording. Figure 11 shows the concentration of the changes within the burst zone, even if small reorganizations persist after the burst. Figure 11a shows the rate of change of the 4 main orders of loops, within the burst area. There is about the same amount of loops created and lost for each type of loop. This means there are reorganizations of the contacts, but the mesoscopic structure remains stable on average and regains a similar structure after bursting (note that the contact force
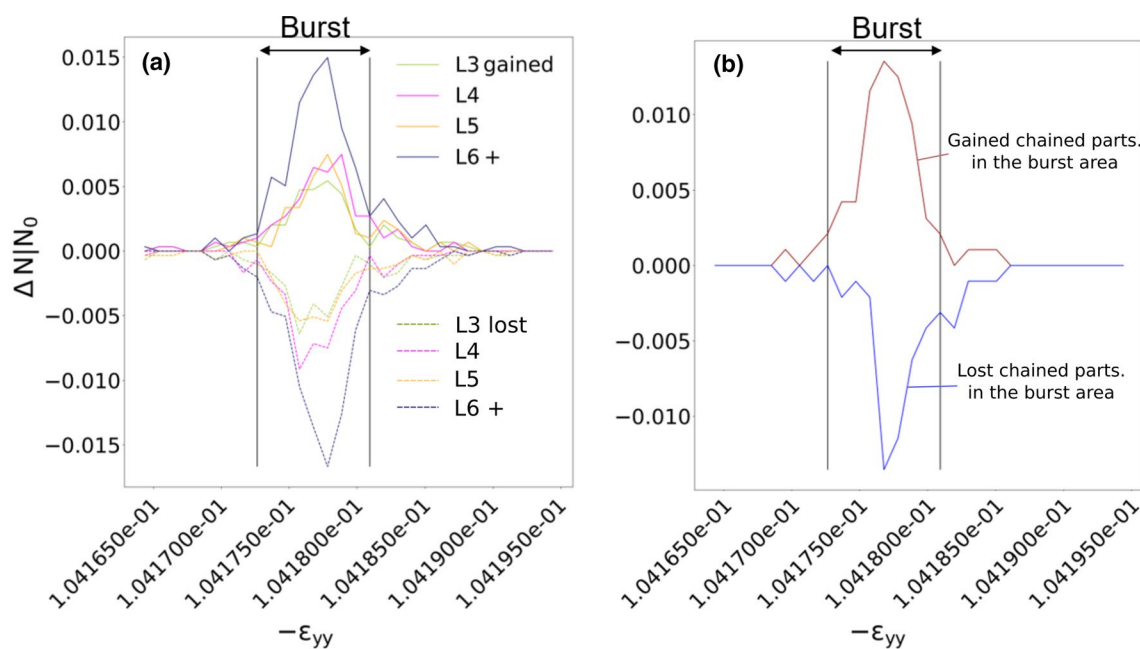
Fig. 11 Relative variation of grain loops (**a**) and rattlers (**b**) in the bounding box domain shown in Fig. 5 (in the vicinity of the burst of kinetic energy)

distribution is modified with less contacts close to sliding). However, we can note that the 3, 4 and 5 order grain loops are broken first (peak of lost loops in the first part of the burst) and then created (peak of gained loops in the second part of the burst). This is not obvious for 6+ order loops, which are the most affected meso-structures. Thus, low order loops are lost and transformed in higher-order loops, while higher-order loops are constantly being created and destroyed to ensure the stability of the sample during an inertial disturbance. Figure 11b shows the evolution of the proportions of new and disappeared rattlers within the bursting zone in relation to the number of rattlers just before the start of the burst. The maximum numbers of gained and lost rattlers are not reached simultaneously. This means that the rattlers are first generated and then lost. This finding is in line with the results obtained with grain loops. Before the peak of kinetic energy, a significant amount of low order loops are lost, which creates rattlers. While kinetic energy decreases, lower-order loops are created by capturing the rattlers. The loss of lower order loops in the first part of the burst (i.e. loops containing little void) is consistent with the existence of local dilatation as raised in Section III.2 and Fig. 6.

Outside the burst zone, no significant trends can be highlighted (Fig. 12). Neither grain loops (Fig. 12a) nor rattlers (Fig 12b) outside the burst zone are altered in number and nature. Figure 12 shows that the location of changes in micro-structures depends on the spatial location of the kinetic energy burst.

Identifying changes at the microscopic scale remains a difficult task, especially since the micro-structure changes are limited and concern a very small fraction of all loops. These limited changes are most likely related to the fact that, in this dense set of grains subjected to a drained biaxial compression, most of the energy is dissipated by friction rather than kinetic energy. However, the meso-domains have made it possible to evidence the changes occurring in the burst zone. Grain loops highlight the microscopic reorganization undergone by the area due to bursting.

5.2 Analysis of the meso-stress

In Fig. 13, each component of the macroscopic stress is compared to the corresponding component of the weighted average sum of all meso-stresses (the loop contributes for its fraction area of the total sample domain). The comparison is made on the whole sample domain and on all the biaxial test long. The dotted lines represent the components of the sum of the meso-stress. They follow very well the evolution of each corresponding macro-component. The proposed definition of a meso-stress is thus sound as it corresponds to the usual macroscopic definition of a stress when weighted average of the meso-stresses is considered.
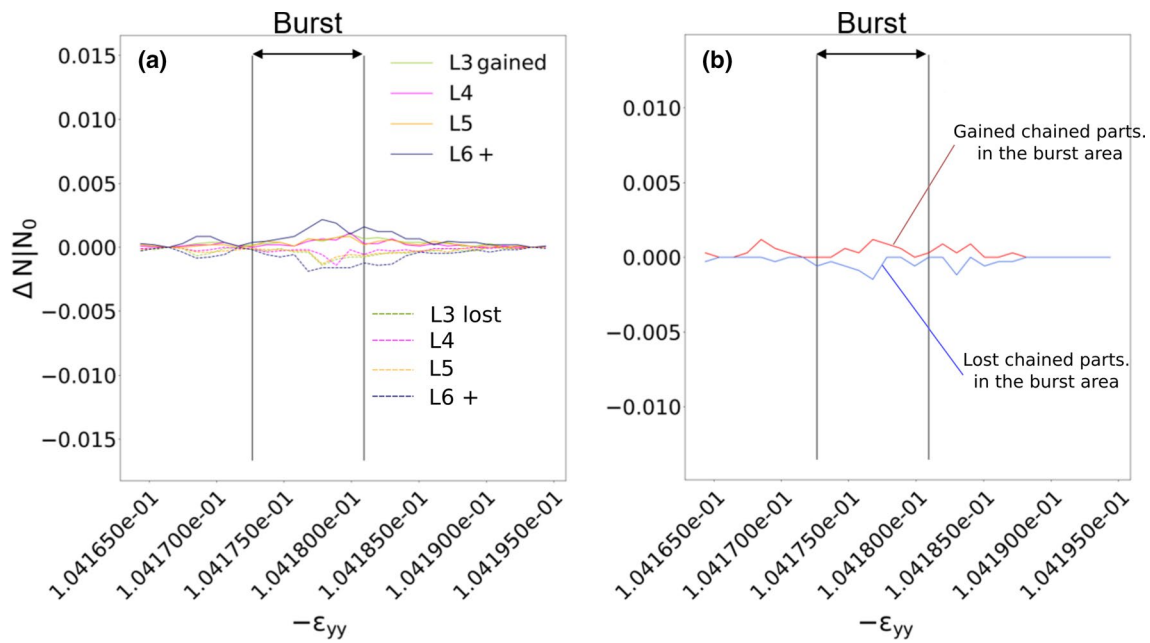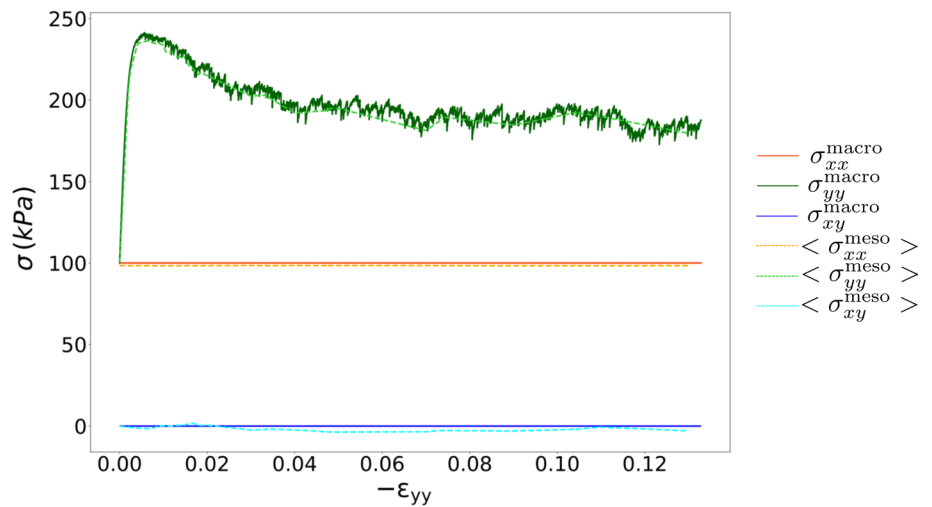
Fig. 12 Relative variation of grain loops (**a**) and rattlers (**b**) outside the bounding box domain shown in Fig. 5 (far from the burst of kinetic energy)

Fig. 13 Comparison between the macroscopic stress σ^{macro} and the volume average of the mesoscopic stress $\langle \sigma^{meso} \rangle$

5.3 Evolution of mesoscopic second-order work during the kinetic energy burst

Figure 14 shows the spatial distribution of mesoscopic second-order works during the propagation of the No. 4 kinetic energy burst. Meso-stress and meso-strain increments are defined on macroscopic increments of axial strain $|\Delta\varepsilon_{yy}| = 10^{-6}$. Thus, each panel in Fig. 14 leads to the same panel of index in Fig. 5, with the exception of the panel (*). The vanishing of mesoscopic second-order work follows the spatial evolution of kinetic energy, with even wider and more detailed limits. Mesoscopic second-order work

reveals some details that cannot be seen simply by looking at kinetic energy. For example, the panel (*) in Fig. 13 is an intermediate step between (a) and (b). In Fig. 5, it can be suggested that the burst appears at the upper center of the sample. However, the panel (*) shows that the instability originates from the lower right corner and propagates to the upper center of the sample. The origin of the burst at the lower right corner is also visible in panel (b) of Fig. 14, but to a lesser extent.

Although maps of second order mesoscopic work seem to reveal more clearly the origins of the kinetic burst, one thing to emphasize is that the whole burst area does
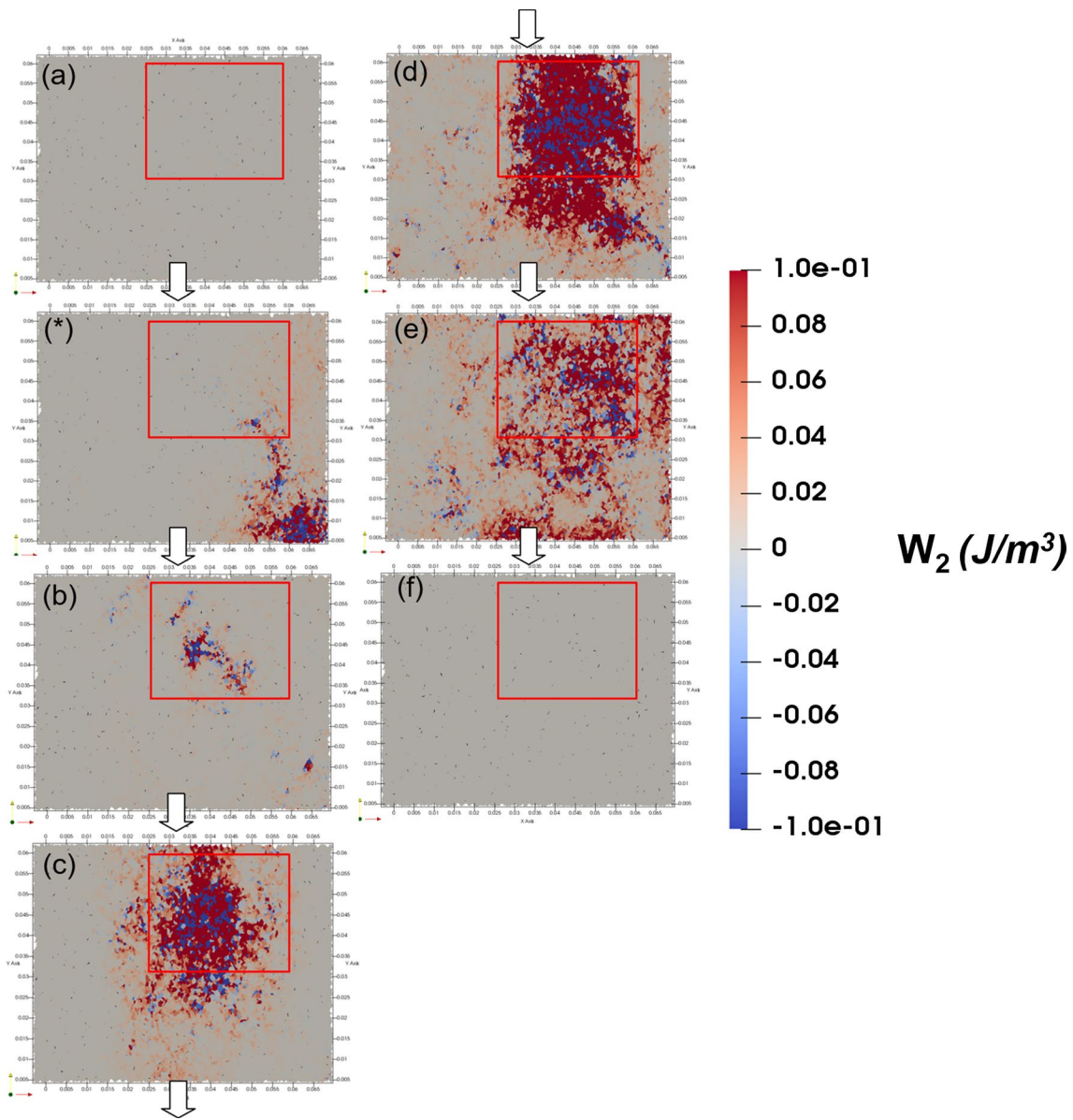
Fig. 14 Reduced time sequence of mesoscopic second-order work W_2 based on the Fig. 7. (**a**) (**b**) (**c**) (**d**) (**e**) (**f**) correspond to the same step of Fig. 7 while (*) corresponds to an additional step between (**a**) and (**b**). A macroscopic axial strain increment $|\varepsilon_{yy}| = 10^{-6}$ is used to compute the incremental meso-strains and meso-stresses. The box delimiting the burst shown in Fig. 5 is reproduced here.

not only have loops with negative second order meso-scopic work. Negative and positive mesoscopic second-order loops are often next to each other. By looking at the volume-weighted average second order work, one can assess the predominance of negative or positive meso-scopic second order work. For the bounding box of the domain Ω_b shown in Fig. 5, the volume-weighted average of the second-order work reads

$$(W_2)_{\Omega_b} = \frac{1}{|\Omega_b|} \sum_l |\Omega_l| (W_2)_{\Omega_l} \qquad (25)$$

The evolution of $\langle W_2 \rangle_{\Omega_b}$ during the outburst of kinetic energy is shown in Fig. 15. $\langle W_2 \rangle_{\Omega_b}$ is negative only at the nucleation of the burst. It then increases to positive values during the burst and then returns to its pre-burst value. The decrease of $\langle W_2 \rangle_{\Omega_b}$ prior to bursting can be seen as a signature of underlying mechanical instability in the bursting domain. The following increase shows that the active reorganizations of the micro-structure that occur during the burst allow for rapid restabilization of the sample and prevent the burst from continuing to grow. As a result, the burst quickly disappears and remains localized. On the other hand, it has been shown by Wautier
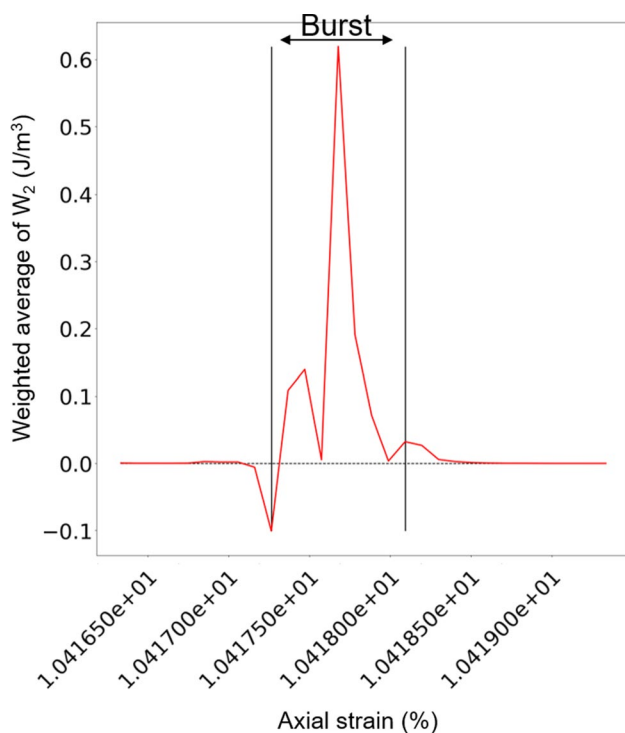
Fig. 15 Volume weighted average of the second-order work during the burst of energy, in the neighbour of the initiation of the burst

et al. [39] that bursts propagating throughout the sample domain are related to mechanical instabilities at the material point scale.

6 Conclusion

In this paper, we have emphasized the importance of meso-domains in the analysis of a burst of kinetic energy that can be observed in granular materials. Changes in grain loops highlight structural displacements at the microscopic scale during bursts. The opening and closing of the grain loops release kinetic energy, while the micro-structure after bursting is very similar to that before, which ensures the statistical equilibrium at critical states. Furthermore, focusing on indicators of inertial transition and mechanical instabilities, we show that the area where the burst occurred contains precursors of kinetic energy release. On the one hand, a large number of contacts with a sliding index close to 1 is required to enable the burst to be triggered in a specific area. On the other hand, the criterion of the second-order work, defined at the mesoscopic scale, predicts the burst of kinetic energy and even gives information on its origins. These results encourage the further use of meso-domains in the study of instabilities. In

the present study, bursts of kinetic energy were observed despite the fact that most of the energy released is directly dissipated through contact friction. The influence of the friction coefficient on the different energies conversion is an aspect that will require additional research work. From a more theoretical point of view, the proposed introduction of a mesoscale attached to meso-structures is based on a number of assumptions that will need to be further investigated to assess their validity where inertial terms could have a larger contribution.

Compliance with ethical standards

Conflict of interest We have no conflicts of interest to disclose.

References

1. Bonelli, S., Millet, O., Nicot, F., Rahmoun, D., De Saxcé, G.: On the definition of an average strain tensor for two-dimensional granular material assemblies. Int. J. Solids Struct. **49**, 947–958 (2012)
2. Bouil Le Amon, A., Sangleboeuf, J.-C., Orain, H., Bésuelle, P., Viggiani, G., Chasle, P., Crassous, J.: A biaxial apparatus for the study of heterogeneous and intermittent strains in granular materials. Granul. Matter **16**, 1–8 (2014)
10. Cambou, B., Jean, M., Radjaï, F.: Micromechanics of granular materials. John Wiley & Sons, London (2013)
3. Cambou, J., Magoariec, H., Nguyen, N.-S.: *Granular Materials at the Meso-scale*. ISTE Press – Elsevier (2016)
4. Darve, F., Servant, G., Laouafa, F., Khoa, H.D.V.: Failure in geomaterials: continuous and discrete analyses. Comput. Methods Appl. Mech. Eng. **193**(27–29), 3057–3085 (2004)
5. Darve, F., Sibille, L., Daouadji, A., Nicot, F.: Bifurcations in granular media: macro-and micro-mechanics approaches. C. R. Méc. **335**(9–10), 496–515 (2007)
6. Forterre, Y., Pouliquen, O.: Flows of dense granular media. Annu. Rev. Fluid Mech. **40**, 1–24 (2008)
7. Gaume, J., Chambon, G., Naaim, M.: Quasistatic to inertial transition in granular materials and the role of fluctuations. Phys. Rev. E **84**(5), 051304 (2011)
8. Gaume, J., Gast, T., Teran, J., van Herwijnen, A., Jiang, C.: Dynamic anticrack propagation in snow. Nat. Commun. **9**(1), 1–10 (2018)
11. Liu, J., Nicot, F., Zhou, W.: Sustainability of internal structures during shear band forming in 2D granular materials. Powder Technol. **338**, 458–470 (2018)
12. Liu, J., Wautier, A., Bonelli, S., Nicot, F., Darve, F.: Macroscopic softening in granular materials from a meso-scale perspective. Int. J. Solids Struct. **193–194**, 222–238 (2020)
13. Marteau, E., Andrade, J.E.: A model for decoding the life cycle of granular avalanches in a rotating drum. Acta Geotechnica **13**(3), 549–555 (2018)
14. Méjean, S., Faug, T., Einav, I.: Discrete Element Method simulations of standing jumps in granular flows down inclines. In EPJ Web of Conferences, EDP Sciences, **140**, 03026 (2017)
9. N Hadda L Sibille F Nicot R Wan F Darve.: Failure in granular media from an energy viewpoint Granul. Matter (2016) https://doi.org/10.1007/s10035-016-0639-8

15. Nguyen, N.S., Magoariec, H., Cambou, B.: Local stress analysis in granular materials at a meso-scale. Int. J. Numer. Anal. Methods Geomech. **36**(14), 1609–1635 (2012)

16. Nguyen, N.S., Magoariec, H., Cambou, B., Danescu, A.: Analysis of structure and strain at the meso-scale in 2D granular materials. Int. J. Solids Struct. **46**(17), 3257–3271 (2009)

17. Nguyen, S.K., Magoariec, H., Vincens, E., Cambou, B.: Towards a new approach for modeling the behavior of granular materials: a mesoscopic-macroscopic change of scale. Int. J. Solids Struct. **97**, 256–274 (2016)

18. Nguyen, N.S., Magoariec, H., Vincens, E., Cambou, B.: On the definition of a relevant meso-scale for upscaling the mechanical behavior of 3D granular materials. Granul. Matter **22**(1), 25 (2020)

19. Nguyen, H.N.G., Prunier, F., Djeran-Maigre, I., Nicot, F.: Kinetic energy and collapse of granular materials. Granul. Matter (2016). https://doi.org/10.1007/s10035-016-0609-1

20. Nicot, F., Darve, F.: A micro-mechanical investigation of bifurcation in granular materials. Int. J. Solids Struct. **44**(20), 6630–6652 (2007)

21. Nicot, F., Hadda, N., Guessasma, M., Fortin, J., Millet, O.: On the definition of the stress tensor in granular media. Int. J. Solids Struct. **50**(14–15), 2508–2517 (2013)

22. Nicot, F., Kruyt, N.P., Millet, O.: On Hill's lemma in continuum mechanics. Acta Mechanica **228**(2), 1581–1596 (2017)

23. Nicot, F., Sibille, L., Darve, F.: Bifurcation in granular materials: an attempt for a unified framework. Int. J. Solids Struct. **46**(22–23), 3938–3947 (2009)

24. Nicot, F., Sibille, L., Darve, F.: Failure in rate-independent granular materials as a bifurcation toward a dynamic regime. Int. J. Plast. **29**, 136–154 (2012)

25. Nicot, F., Xiong, H., Wautier, A., Lerbet, J., Darve, F.: Force chain collapse as grains column buckling in granular materials. *Granul. Matter*, **19**(2) (2017)

26. Peng, C., Guo, X., Wu, W., Wang, Y.: Unified modelling of granular media with smoothed particle hydrodynamics. Acta Geotechnica **11**(6), 1231–1247 (2016)

27. Peters, J.F., Muthuswamy, M., Wibowo, J., Tordesillas, A.: Characterization of force chains in granular material. Phys. Rev. E **72**(4), 041307 (2005)

28. Radjai, F., Jean, M., Moreau, J.J., Roux, S.: Force distributions in dense two-dimensional granular systems. Phys. Rev. Lett. **77**(2), 274 (1996)

29. Sibille, L., Villard, P., Darve, F., Aboul Hosn, R.: Quantitative prediction of discrete element models on complex loading paths. Int. J. Numer. Anal. Methods Geomech. **43**(5), 858–887 (2019)

31. Staron, L., Radjai, F., Vilotte, J.P.: Multi-scale analysis of the stress state in a granular slope in transition to failure. Eur. Phys. J. E **18**(3), 311–320 (2005)

32. Staron, L., Vilotte, J.P., Radjai, F.: Preavalanche instabilities in a granular pile. Phys. Rev. Lett. **89**(20), 204302 (2002)

33. Tordesillas, A.: Force chain buckling, unjamming transitions and shear banding in dense granular assemblies. Philos. Mag. **87**(32), 4987–5016 (2007)

34. Vescovi, D., Berzi, D., di Prisco, C.: Fluid–solid transition in unsteady, homogeneous, granular shear flows. Granul. Matter **20**(2), 27 (2018)

35. Walker, D.M., Tordesillas, A., Froyland, G.: Mesoscale and macroscale kinetic energy fluxes from granular fabric evolution. Phys. Rev. E **89**(3), 032205 (2014)

36. Wan, R., Nicot, F., Darve, F.: Failure in Geomaterials A Contemporary Treatise. ISTE Press Elsevier, London (2017)

37. Wautier, A., Bonelli, S., Nicot, F.: Scale separation between grain detachment and grain transport in granular media subjected to an internal flow. Granul. Matter **19**(2), 22 (2017)

38. Wautier, A., Bonelli, S., Nicot, F.: Flow impact on granular force chains and induced instability. Phys. Rev. E **98**(4), 042909 (2018)

39. Wautier, A., Bonelli, S., Nicot, F.: Micro-inertia origin of instabilities in granular materials. Int. J. Numer. Anal. Methods Geomech. **42**(9), 1037–1056 (2018)

40. Welker, P., McNamara, S.: Precursors of failure and weakening in a biaxial test. Granul. Matter **13**, 93–105 (2011)

41. Yan, B., Regueiro, R.A.: Definition and symmetry of averaged stress tensor in granular media and its 3D DEM inspection under static and dynamic conditions. Int. J. Solids Struct. **161**, 243–266 (2019)

42. Zhu, H., Nicot, F., Darve, F.: Meso-structure evolution in a 2D granular material during biaxial loading. Granul. Matter **18**(1), 3 (2016)

30. Šmilauer, V., et al.: Yade reference documentation. *Yade Documentation*, **474**(1) (2010)